Journal of Hazardous Materials 213–214 (2012) 193–199

Contents lists available at SciVerse ScienceDirect

Journal of Hazardous Materials

journal homepage: www.elsevier.com/locate/jhazmat

Ultrasensitive fluorescence-quenched chemosensor for Hg(II) in aqueous solution based on mercaptothiadiazole capped silver nanoparticles

N. Vasimalai, G. Sheeba, S. Abraham John*

Department of Chemistry, Gandhigram Rural Institute, Gandhigram, 624 302 Dindigul, Tamilnadu, India

ARTICLE INFO

Article history:
Received 28 November 2011
Received in revised form 24 January 2012
Accepted 24 January 2012
Available online 2 February 2012

Keywords:
Chemosensor
Mercuric ions
2,5-Dimercapto-1,3,4-thiadiazole
Silver nanoparticles
Water samples

ABSTRACT

This manuscript describes a highly selective and ultra sensitive determination of Hg(II) in aqueous solution using functionalized mercaptothiadiazole capped silver nanoparticles (AgNPs) by spectrofluorimetry. We have synthesized 2,5-dimercapto-1,3,4-thiadiazole (DMT), 2-mercapto-5-methyl-1,3,4-thiadiazole (MMT) and 2-mercapto-5-amino-1,3,4-thiadiazole (AMT) capped AgNPs by wet chemical method. Among these AgNPs, DMT capped AgNPs (DMT-AgNPs) were more stable and highly fluorescent than the other two AgNPs. DMT-AgNPs show the emission maximum at 677 nm while exciting at 400 nm. After the addition of Hg(II), the emission intensity was decreased at 677 nm. The observed decreased emission intensity was ascribed to the aggregation of AgNPs and it was confirmed by TEM. Based on the decrease in emission intensity, the concentration of Hg(II) was determined. The lowest detection limit (LOD = 3 S/m) of 1.0 pg L^{-1} was achieved for the first time using DMT-AgNPs by spectrofluorimetry. The quantum yield (ϕ_F), Stern–Volmer constant (K_{SV}), Gibbs free energy changes (ΔG°), association constant (K_f) were calculated and the quenching mechanism also was discussed. Finally, the proposed method was successfully utilized for the determination of Hg(II) in river water, industrial effluent water and tap water samples. The obtained results were fairly matches with the ICP-AES method.

1. Introduction

Metal nanoparticles based research has received great attention during the last three decades due to their attractive optical, catalytic and electrical properties [1,2]. These unique properties can be tuned by varying the particle size, shape and surrounding environments [3]. When compared to other metal nanoparticles, research on the synthesis and applications of silver nanoparticles (AgNPs) has received considerable attention around the world in recent years [4,5]. The AgNPs show excellent conductivity, chemical stability and catalytic activity [6,7]. They have been used extensively as an antibacterial agent, food storage, textile coatings and toxic chemicals sensor [8].

Toxic heavy metal ions can cause lethal threat to the environment and human beings. Among them, mercury has received much attention due to its high toxicity and bioaccumulative properties [9,10]. Mercury contamination arises from a variety of natural sources, such as oceanic and volcanic emissions, as well as anthropogenic sources, such as gold mining and combustion of wastes and fossil fuels are the major sources of mercury emission [11]. Bioaccumulation of mercury can affect brain, heart, stomach and intestines [12]. Hg(II) shows strong affinity towards the ligands containing sulfur group and causes the blocking of sulfydryl groups of proteins, enzymes, membranes and it damage to the central nervous system, DNA, mitosis and the endocrine system [13]. According to Environmental Protection Agency and World Health Organization guidelines, Hg(II) must be in the concentrations of 2 ppm and 5 ppm in drinking water, respectively [14,15]. Because of its serious hazardous effects to human health and environment, there is a strong need to establish a simple inexpensive method to determine Hg(II) with high selectivity and sensitivity in aqueous media. Many methods have been described in the literature for the determination of Hg(II) including colorimetry [16,17], spectrophotometry [18], atomic absorption spectrometry [19], stripping voltammetry [20] and inductively coupled plasma atomic emission spectrometry [21]. Among the different methods, spectrofluorimetric method has several advantages over other methods which include higher sensitivity, selectivity and reproducibility and less time consumption [22,23]. To date only few papers were reported for the determination of Hg(II) in ppt level by spectrofluorimetric method [7,10,24–35].

The present work describes the ultrasensitive fluorescence-quenched chemosensor for Hg(II) in aqueous solution using mercaptothiadiazole capped AgNPs as a fluorophore. We have

* Corresponding author. Tel.: +91 451 245 2371; fax: +91 451 245 3031.
E-mail address: abrajohn@yahoo.co.in (S.A. John).

0304-3894/$ – see front matter © 2012 Elsevier B.V. All rights reserved.
doi:10.1016/j.jhazmat.2012.01.079

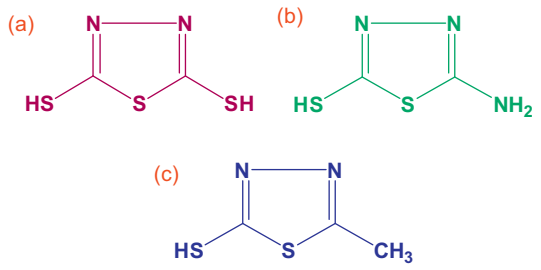

Chart 1. Structure of (a) 2,5-dimercapto-1,3,4-thiadiazole (DMT), (b) 2-amino-5-mercapto-1,3,4-thiadiazole (AMT) and (c) 2-methyl-5-mercapto-1,3,4-thiadiazole (MMT).

synthesized 2,5-dimercapto-1,3,4-thiodiazole (DMT), 2-amino-5-mercapto-1,3,4-thiadiazole (AMT) and 5-methyl-2-mercapto-1,3,4-thiodiazole (MMT) (Chart 1) capped AgNPs by wet chemical method. The synthesized AgNPs were characterized by UV–vis spectrophotometer, spectrofluorimeter, HR-TEM, FT-IR and XRD. The DMT-AgNPs are more stable and highly fluorescent than the other two AgNPs. Therefore, we have chosen DMT-AgNPs for the determination of Hg(II). They show the emission maximum at 677 nm while exciting at 400 nm. The emission intensity was decreased while adding Hg(II) to DMT-AgNPs. Based on decrease in emission intensity the concentration of Hg(II) was determined. The lowest detection limit was found to be 1.0 pg L^{-1}. The present method was successfully applied to determine Hg(II) in environmental samples. The obtained results have a good agreement with ICP-AES method.

2. Experimental

2.1. Chemicals

Silver nitrate, 2,5-dimercapto-1,3,4-thiodiazole, 2-amino-5-mercapto-1,3,4-thiadiazole, 5-methyl-2-mercapto-1,3,4-thiodiazole were purchased from Sigma-Aldrich. Sodium borohydride ($NaBH_4$) and mercuric nitrate ($Hg(NO_3)_2$) were purchased from Merck (India) and were used as received. All other chemicals used in this investigation were of analytical grade and used directly without further purification. Double distilled water was used to prepare the solutions in the present work.

2.2. Instrumentation

Absorption spectra were measured by using JASCO V-550 UV–vis spectrophotometer. Fluorescence spectral measurements were performed on a JASCO FP-6500 spectrofluorimeter equipped with a xenon discharge lamp, 1 cm quartz cell at room temperature. The FT-IR spectra of the solid AgNPs were measured by using JASCO 460 plus FT-IR Spectrophotometer. High resolution transmission electron microscopy (HR-TEM) images of AgNPs were obtained from a JEOL JEM 3010 operating at 200 kV. For TEM measurements, the sample was prepared by dropping 2 μL of a AgNPs colloidal solution onto a carbon-coated copper grid. A large volume (250 mL) of DMT-AgNPs was synthesized and centrifuged (10,000 rpm) and the particles were separated. They repeatedly washed with water and dried in vacuum. The dried AgNPs powder was used for XRD and FT-IR measurements. XRD analysis was carried out with a Rigaku X-ray diffraction unit using Ni-filtered Cu Kα (λ = 1.5406) radiation. Inductively coupled plasma atomic emission spectra (ICP-AES) were measured by using thermo electron IRIS intrepid II XSP DUO model ICP-AES.

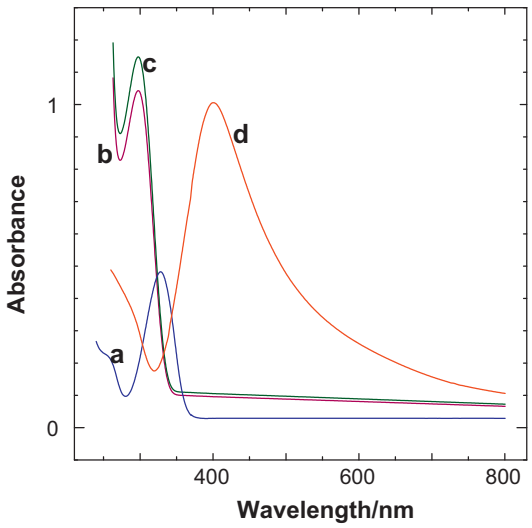

Fig. 1. Absorption spectra obtained for (a) DMT, (b) $AgNO_3$ and after the addition (c) $AgNO_3$ to DMT and (d) $NaBH_4$ to a mixture of $AgNO_3$ and DMT.

2.3. Synthesis of functionalized mercaptothiadiazole ligand capped AgNPs

All glasswares were thoroughly cleaned with freshly prepared aquaregia (3:1; HCl/HNO_3) and rinsed comprehensively with double distilled water prior to use. The colloidal solution of mercaptothiodiazole capped AgNPs were prepared by the following procedure. 2 mL of $AgNO_3$ (1 mM) and 1 mL of DMT (1 mM) were added to 92 mL of water in a round bottom flask with constant stirring. To this solution, 5 mL of 0.046 M $NaBH_4$ was added drop by drop and the stirring was continued for another 30 min. The color of the solution turns into yellow immediately after the final addition, indicating the formation of AgNPs. Same procedure was followed for the preparation of AMT and MMT-AgNPs using 0.5 mM of the respective compound.

3. Results and discussion

3.1. Silver nanoparticles formation and stability

Since metal nanoparticles exhibit strong absorption band due to surface plasmon resonance (SPR) in the visible region, the electronic spectroscopy is one of the simplest techniques to characterize them. Fig. 1 shows the absorption spectra recorded for DMT, $AgNO_3$ and a mixture of DMT and $AgNO_3$ in the presence and absence of $NaBH_4$. DMT shows an absorption maximum at 318 nm with a shoulder band around at 260 nm (curve a). $AgNO_3$ in water exhibits an absorption maximum at 300 nm (curve b). Addition of $AgNO_3$ solution to an aqueous solution of DMT causes the absorption bands characteristics of DMT to vanish while the absorption intensity at 300 nm was increased (curve c). The observed increase in intensity at 300 nm was ascribed to the complex formation between DMT and $AgNO_3$. When 5.0 mL of 0.046 M of $NaBH_4$ was slowly added to a mixture of DMT and $AgNO_3$ solution, the colorless solution becomes yellow immediately and shows a new absorption band at 400 nm (curve d), corresponding to SPR. The observed SPR band at 400 nm confirms the successful formation of AgNPs. Similar procedure was used to prepare AMT- and MMT-AgNPs. The AMT and MMT-AgNPs show SPR bands at 404 and 396 nm, respectively.

The stability of the metal nanoparticles was usually checked from the changes in their absorption characteristics such as shift in the absorption maximum and decrease in the absorbance. Fig .S1A (Supporting information) shows the absorption spectra

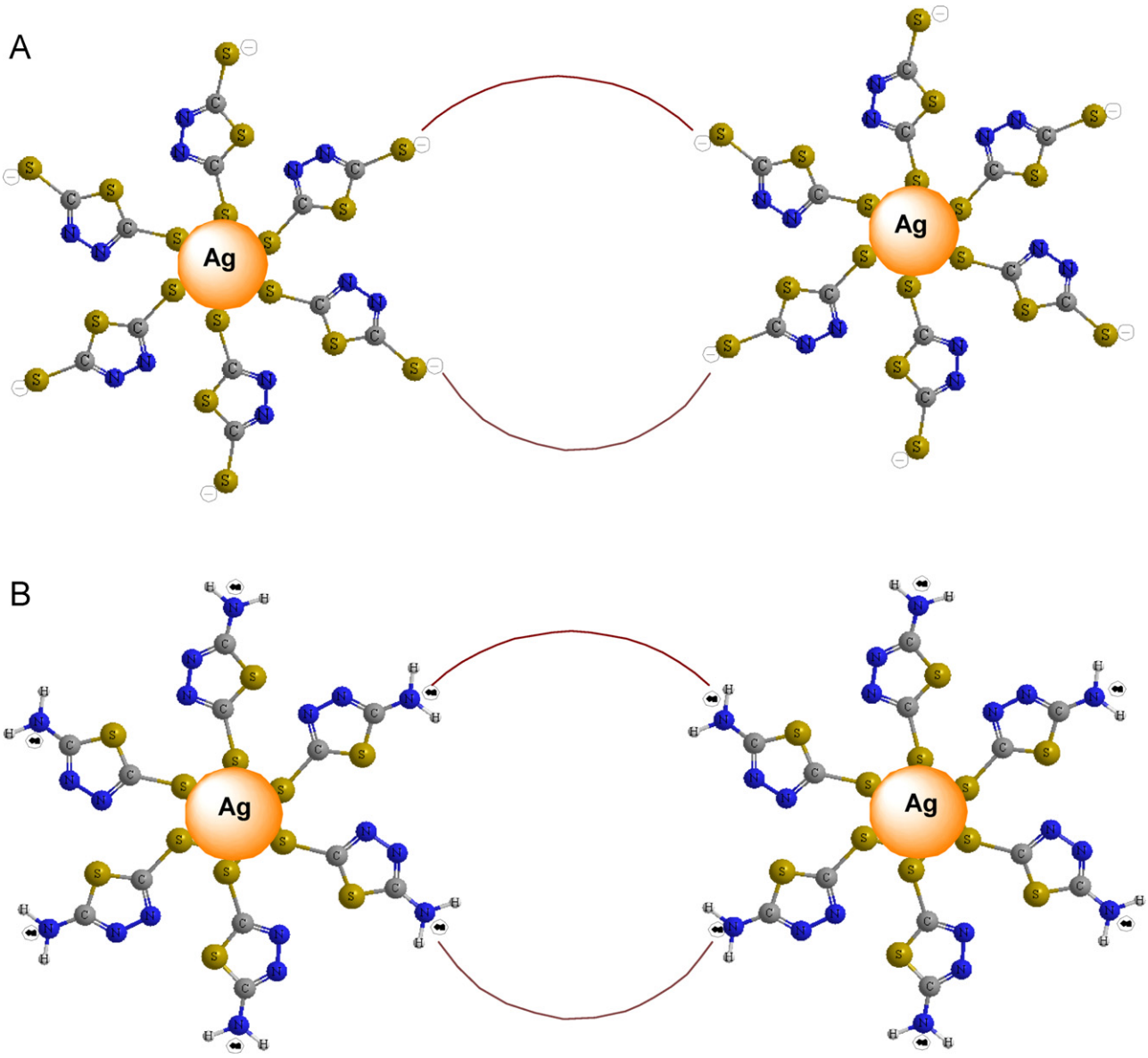

Scheme 1. Schematic representation of AgNPs stabilized by (A) DMT and (B) AMT.

obtained for freshly prepared DMT-AgNPs and three months aged solution. As can be seen from curve b, except a marginal decrease in the absorbance no shift in the absorption maximum was observed for three months old DMT-AgNPs solution when compared to freshly prepared solution (curve a). This shows that the DMT-AgNPs were highly stable. Very similar absorption characteristics were also observed for AMT-AgNPs (Fig. S1B (Supporting information)). During the formation of DMT-AgNPs, it is expected that one of the thiolate groups of DMT chemisorbed on AgNPs while the other thiolate group is pointing away from the AgNPs surface and stabilized the AgNPs by strong electrostatic repulsion (Scheme 1A). In addition to thiolate species, it is also expected that the lone pair of electrons of nitrogen in the ring can also stabilize the AgNPs.

In the case of AMT, the thiolate groups were attached with the AgNPs while the amino groups are projecting away from the AgNPs surface. It is likely that the lone pair of electrons present in the amino groups stabilize the AgNPs by electrostatic repulsion (Scheme 1B). Unlike DMT- and AMT-AgNPs, the stability of MMT-AgNPs is very poor. The absorption spectrum recorded for 10 days old MMT-AgNPs shows not only decrease in the absorbance but also a small shift in the absorption maximum (Fig. S1C (Supporting information)) [36,37]. After a month, a precipitate was settled down at the bottom of the beaker due to aggregation. The observed poor stability of MMT-AgNPs was ascribed to the absence of strong electrostatic repulsion on the surface of the AgNPs.

3.2. Characterization of AgNPs by TEM, XRD and FT-IR studies

The size and morphology of the AgNPs were examined by TEM. Fig. 2 shows the TEM image of DMT-AgNPs. The TEM image of DMT-AgNPs shows that they are roughly spherical in shape with a size of ~5 nm. The crystalline nature of AgNPs was also confirmed from the XRD analysis (Fig. S2 (Supporting information)). It shows the DMT-AgNPs diffraction features appearing at 37.17°, 44.37°, 66.62° and 77.47° corresponding to (1 1 1), (2 0 0), (2 2 0) and (3 1 1), respectively [38]. Among the different planes, the peak corresponding to the (1 1 1) plane is more intense than the other planes. The ratio between the intensity of the (2 0 0) and (1 1 1) diffraction peaks

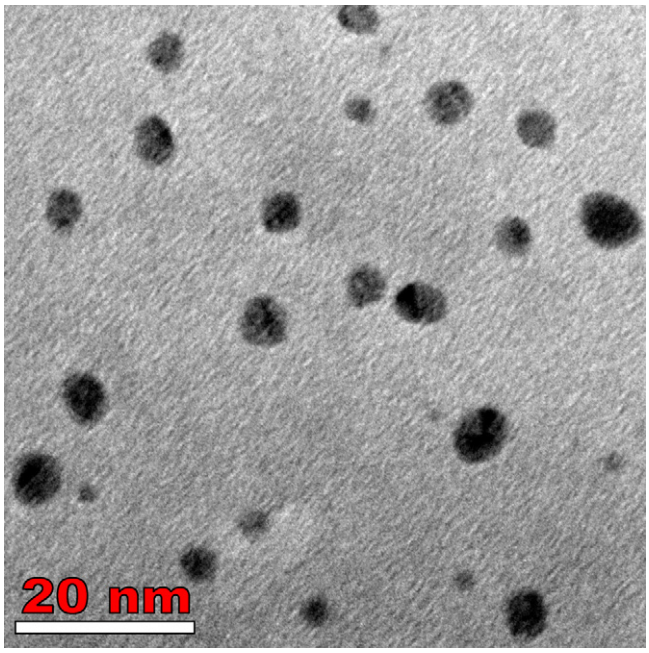

Fig. 2. TEM image of DMT-AgNPs.

was much lower (0.5), suggesting that the (1 1 1) plane is predominant orientation. The width of the (1 1 1) peak was employed to calculate the average crystalline size of the DMT-AgNPs using the Scherrer equation [38]. The calculated average size of the AgNPs is ~6.0 nm, which matches with the particle size obtained from TEM image.

Further, capping of the ligands with AgNPs was confirmed by FT-IR measurements. The FT-IR spectra obtained for the solid DMT and DMT-AgNPs are shown in Fig. S3 (Supporting information). The bands obtained for solid DMT in the region of 3100–2500 cm^{-1} (curve a) were also observed for DMT-AgNPs with slight shift and less intensity (curve b). While in the region of 1500–800 cm^{-1}, many bands were absent for DMT-AgNPs when compared to solid DMT (curve b). The appearance of very weak band at 2358 cm^{-1} for DMT-AgNPs suggests the presence of free–SH groups on the surface of AgNPs (curve b) [39]. The different spectral bands and their assignments for solid DMT and DMT-AgNPs are given in Table S1 (Supporting information).

3.3. Determination of Hg(II) by spectrophotometry

The absorption spectra of DMT-AgNPs in the presence of different concentrations of Hg(II) are shown in Fig. 3. The colloidal solution of DMT-AgNPs shows the SPR band at 400 nm (curve a). The intensity of this band and a small shoulder band at 270 nm were decreased dramatically while adding Hg(II) into DMT-AgNPs (curves b–h). The observed decrease in absorbance may be due to aggregation of AgNPs. Interestingly two well defined isosbestic points were appeared at 280 and 350 nm (Fig. 3), confirming a neat interconversion between dispersed DMT-AgNPs and aggregated DMT-AgNPs. The colloidal solution of DMT-AgNPs displays a yellow color (Fig. 3; Inset: A). The yellow color solution was slowly changes into colorless solution while increasing the concentration of Hg(II). After the addition of 70 μM Hg(II), a highly intense yellow color DMT-AgNPs was changed into colorless solution (Fig. 3; inset B). Further increasing the concentration of Hg(II) leads to complete aggregation of AgNPs which was settled down at the bottom of the quartz cell. The absorption spectra of DMT-AgNPs in the presence of nanomolar concentrations of Hg(II) do not show any significant changes at 270 and 400 nm unlike micromolar

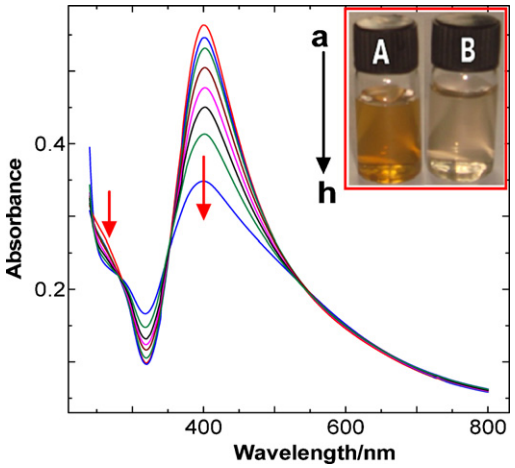

Fig. 3. Absorption spectra of DMT-AgNPs after the addition of (a) 0, (b) 10, (c) 20, (d) 30, (e) 40, (f) 50, (g) 60 and (h) 70 × 10^{-6} mol L^{-1} Hg(II). *Inset:* Photographs of (A) DMT-AgNPs and (B) 70 × 10^{-6} mol L^{-1} Hg(II) in DMT-AgNPs.

concentrations of Hg(II). Further, no visible color change was also observed after the addition of nanomolar Hg(II) to DMT-AgNPs solution. Thus, spectrophotometric method is not suitable to determine low concentration of Hg(II) using DMT-AgNPs.

3.4. Fluorescence spectral studies

The fluorescence spectra of DMT-AgNPs in the presence of different concentrations of Hg(II) are shown in Fig. 4. The fluorescence spectrum of DMT-AgNPs shows emission maximum at 677 nm with an excitation wavelength of 400 nm (curve a). The emission intensity at 677 nm was dramatically decreased while increasing the concentration of Hg(II) (curve b–l). Interestingly, even in the presence of 1.0 pM Hg(II), the emission intensity at 677 nm was decreased (curve b). The observed decrease in emission intensity was mainly due to the aggregation of DMT-AgNPs. This was further confirmed by TEM studies. The TEM image obtained for DMT-AgNPs before and after the addition of 70 μM Hg(II) are shown in Fig. 5.

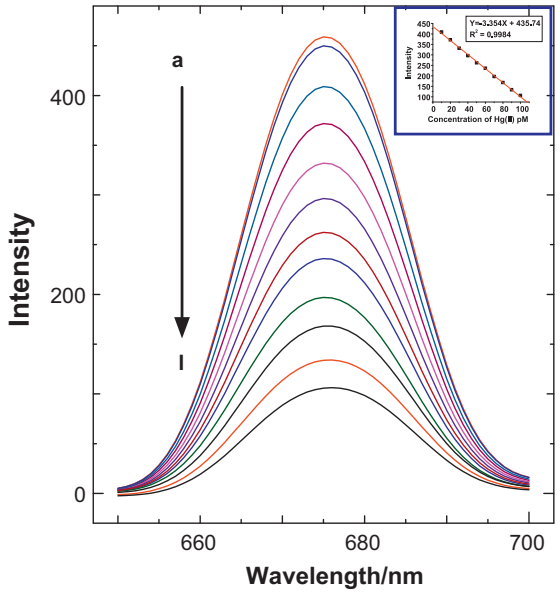

Fig. 4. Fluorescence spectra of DMT-AgNPs after the addition of (a) 0, (b) 1, (c) 10, (d) 20, (e) 30, (f) 40, (g) 50, (h) 60, (i) 70, (j) 80, (k) 90 and (l) 100 × 10^{-12} mol L^{-1} Hg(II). *Inset:* calibration plot for DMT-AgNPs in 10–100 × 10^{-12} mol L^{-1} of Hg(II) (λ_{ex}: 400 nm, λ_{em}: 677 nm).

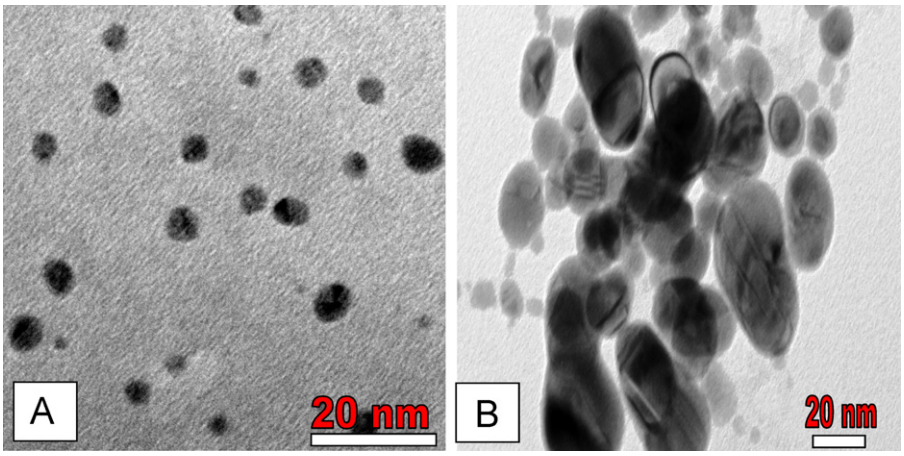

Fig. 5. TEM images of DMT-AgNPs before (A) and (B) after the addition of 70 μM Hg (II).

As can be seen from Fig. 5, after the addition of 70 μM Hg(II), the AgNPs were aggregated and the diameter of each aggregate was ~30 nm.

According to Mie theory, when the distance between two nanoparticles becomes smaller than the sum of their radii, the SPR band becomes broaden and decreased absorbance and emission intensities [39,40]. Both absorbance and emission spectral results were in good agreement with the Mie theory (Fig. 3 and Fig. 4). A good linearity was observed in the emission intensity against 10–100 pM concentrations of Hg(II) ($R^2 = 0.9984$). The detection limit was found to be 1.0 pg L^{-1}. The detection limit obtained in the present method was compared with the previous reports and are given in Table 1. Compared to previous methods, the lowest detection limit was obtained for Hg(II) by the present method.

3.5. Determination of quantum yield

The determination of quantum yield is generally accomplished by a comparison of the wavelength – integrated intensity of the unknown sample with the standard. Fluorescent quantum yield values (ϕ_F) of DMT-AgNPs and DMT-AgNPs in the presence of Hg(II) were calculated by using the comparative William's method [41]. For this purpose, we used quinine sulfate as reference quantum yield standard. The integrated fluorescence intensities of DMT-AgNPs and Hg(II) aggregated DMT-AgNPs were plotted versus absorbance for the reference standard. The gradients of the plot are proportional to the quantity of quantum yield of the standard molecules. The ϕ_F value was calculated according to Eq. (1).

$$\phi_{F(X)} = \left(\frac{\mathrm{Grad_X}}{\mathrm{Grad_{ST}}}\right)\left(\frac{n_X^2}{n_{ST}^2}\right) \quad (1)$$

where "ST" and "X" denote standard and sample, respectively. "Grad" is the gradient from the plot and "n" is the refractive index of the solvent (water). According to the data, fluorescence quantum yield of DMT-AgNPs and Hg(II) aggregated DMT-AgNPs was found to be 0.7312 and 0.2106, respectively. The addition of Hg(II) to DMT-AgNPs decreases the emission intensity and thereby decreases the quantum yield.

3.6. Quenching mechanism, Stern–Volmer and association constants

The quenching constant (K_{SV}) can be calculated by using Stern–Volmer equation given below [42].

$$\frac{F_0}{F} = 1 + K_{SV}[Q] \quad (2)$$

where "F" is the fluorescence intensity of DMT-AgNPs in the presence of Hg(II) and "F_0" is the fluorescence intensity of dispersed DMT-AgNPs. "K_{SV}" is the Stern–Volmer quenching constant and "[Q]" is the concentration of Hg(II). The Stern–Volmer plot F_0/F versus [Q] showed a positive deviation (Fig. S4 (Supporting information)). The obtained Stern–Volmer plot is curve in nature and K_{SV} was found to be 3.1709×10^{10} L mol^{-1}. The positive deviation was observed at higher concentrations of Hg(II), it may be due to the simultaneous presence of dynamic and static quenching mechanisms [42,43]. The obtained Stern–Volmer constant value suggests that there is strong fluorescence quenching between DMT-AgNPs and Hg(II).

The fraction of Hg(II) bound to the DMT-AgNPs (θ) was determined using the following equation [44]

$$\theta = \frac{F_0 - F}{F_0} \quad (3)$$

From the value of "θ", the association constant K_f can be calculated by using the following equation [45]

$$\left(\frac{1}{1-\theta}\right) K_f = \frac{[\mathrm{Hg(II)}]}{\theta} - n[\mathrm{AgNPs}] \quad (4)$$

where n is the number of binding sites, [Hg(II)] is the concentrations of Hg(II) and [AgNPs] is the concentration of DMT-AgNPs. From the plot of $1/(1-\theta)$ versus $[\mathrm{Hg(II)}]/\theta$, the value of K_f was calculated. It was found to be 1.2916×10^{11} mol L^{-1}. The standard Gibbs free energy change (ΔG° was calculated from the K_f using the relation $\Delta G^\circ = -2.303RT \log_{10} K_f$) was found to be −63 kJ. This result indicates that the interactions between Hg(II) and DMT-AgNPs are spontaneous.

3.7. Effect of foreign ions

The effect of various metal ions on the determination of Hg(II) was investigated by analyzing the sample solutions containing 100 nM Hg(II). Interfering ions including cations and anions of 50,000 fold concentration (5 mM) were added into DMT-AgNPs containing 100 nM Hg(II) to find the selectivity. As shown in Fig. 6, DMT-AgNPs selectively aggregate with Hg(II) in the presence of several metal ions. It is to be noted that the presence of 50,000 fold concentration of Pb(II) and EDTA interferes on the determination of Hg(II). However, no interference was observed in the presence of 5000 and 2000 fold Pb(II) and EDTA, respectively. Thus, Hg(II) can be selectively determined in the presence of 50,000 fold of common anions Cl^-, SO_4^{2-}, NO_3^- and common cations, Na^+, K^+, Mg^{2+}, Ca^{2+}, Fe^{2+}, Cu^{2+}, Cd^{2+}, Cr^{3+}, Mn^{2+}, Fe^{3+}, Zn^{2+}, Co^{2+}, Ni^{2+}, and 5000 and 2000 fold $Pb^{2+}$and EDTA, respectively (Fig. 6).

Table 1
Comparison of Hg(II) detection limit, medium, linear range and major interferents obtained in the present study with the reported fluorophores by fluorimetry method.

S. no	Fluorophore	Medium	Linear range	Detection limit	Major interferent	Reference
1	Dihydroxy lipoic acid-AgNC	Water	0.01–10 μM	19.4 ng	–	[7]
2	Rhodamine hydrazone derivative	Acetonitrile	0.001–1 μM	0.8 μg	–	[26]
3	Mercapto acetic acid-CdS	Water	0.005–0.4 μM	0.8 μg	Cu^{2+}, Ag^{+}	[27]
4	Porpyrine-$AuSiO_2$ NPs	Water	1–5 μM	1.2 μg	–	[29]
5	Cyclodextrin-AuNPs	DMF/acetic acid	1–10 nM	9.5 ng	Ag^{+}	[30]
6	Cysteine-AgNPs	Water	0–30 μM	48.4 μg	–	[31]
7	Rhodamine-Fe_3O_4@SiO_2	Acetonitrile	2.7–7.45 mM	23.0 μg	–	[32]
8	Coreshell-SiNPs	Ethanol/water	10–100 μM	1.9 mg	Cu^{2+}	[33]
9	AuNC	Water	1–20 nM	96.9 ng	–	[34]
10	DMT-AgNPs	Water	10–100 pM	1.0 pg	Pb^{2+}, EDTA	This work

Table 2
Determination of Hg(II) in different water samples ($n = 5$).

Samples	Hg(II) added (ng L^{-1})	Hg(II) found (ng L^{-1})	R.S.D.	Recovery (%)
I.E. water	–	80.00 ± 0.60	1.21	104.5
	20	103.11 ± 1.16	0.86	98.8
	30	115.60 ± 1.03	1.05	99.6
River water	–	–	–	–
	20	20.02 ± 0.24	1.41	98.7
	30	30.03 ± 0.18	0.98	99.5
Tap water	–	–	–	–
	20	20.00 ± 0.11	0.84	98.2
	30	30.01 ± 0.39	0.96	102.4

I.E. water = industrial effluent water.

Table 3
Comparison of the present method of determination of Hg(II) with the ICP-AES method.

Hg(II) added (mg L^{-1})	Hg(II) found (mg L^{-1})		R.S.D.
	Fluorimetry method (this work)	ICP-AES method	
0.05	0.050 ± 06	0.054 ± 03	98.3
0.1	0.106 ± 04	0.108 ± 02	100.2

It has been already reported that Hg(II) exhibits stronger thiophilic tendency when compared to other competing heavy metal ions including Pb(II), Cd(II) and Cu(II) [24,46,47]. Thus, Hg(II) selectively binds with DMT-AgNPs even at low concentration in the presence of high concentrations of other ions. Upon the addition of Hg(II), the terminal sulfur atom of DMT-AgNPs establishes strong coordination bond with Hg(II) besides nitrogen atom, resulting the aggregation of DMT-AgNPs via bridging of neighboring nanoparticles (Supporting Information Scheme S1) [10]. Another probable reason for the aggregation is the decrease in the degree of electrostatic repulsion between each AgNPs due to the binding of Hg(II) with terminal sulfur atom of DMT-AgNPs [48].

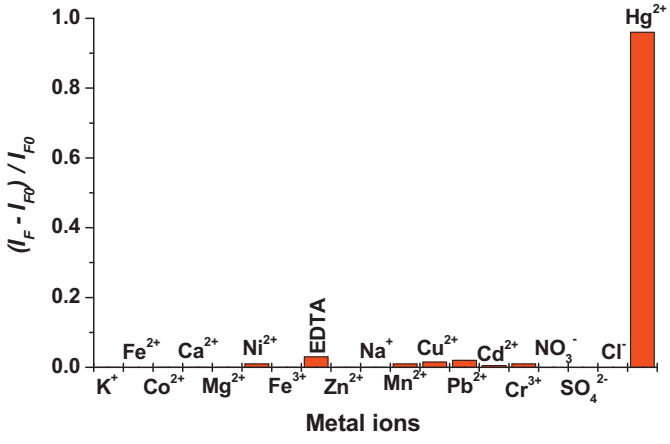

Fig. 6. Selectivity of the DMT-AgNPs towards Hg(II). The emission response of Hg(II) (100×10^{-9} mol L^{-1}) containing DMT-AgNPs in the presence of 5.0×10^{-3} mol L^{-1} of Na^{+}, K^{+}, Mg^{2+}, Ca^{2+}, Fe^{2+}, Cu^{2+}, Cd^{2+}, Cr^{3+}, Mn^{2+}, Fe^{3+}, Zn^{2+}, Co^{2+}, Ni^{2+}, Cl^{-}, SO_4^{2-}, NO_3^{-}, 0.5×10^{-3} mol L^{-1} Pb^{2+} and 0.2×10^{-3} mol L^{-1} EDTA.

3.8. Practical applications

The application of the proposed method was evaluated by determining Hg(II) in river water, industrial effluent water and tap water samples. The obtained results are given in Table 2. The results obtained by the present method have a good agreement with the results obtained from ICP-AES method (Table 3). The lowest detection capacity of ICP-AES is 0.05 mg L^{-1}. The water samples collected from river, industrial effluent and tap were used without previous treatment and known amounts of Hg(II) were spiked with a standard stock solution. The recovery of 98.2% and 104.5% were obtained and good agreement and Hg(II) was obtained between spiked and measured analyte amounts.

4. Conclusion

In the present work, synthesis of functionalized mercaptothiadiazole (DMT, AMT and MMT) capped AgNPs carried out by wet chemical method. Among the AgNPs, DMT-AgNPs show more fluorescent and highly stable. The emission intensity of DMT-AgNPs was decreased at 677 nm, while adding Hg(II). It was ascribed due to the aggregation of AgNPs and it was confirmed by TEM. Based on the decrease in emission intensity, the concentration of Hg(II) was determined. The lowest detection limit 1.0 pg L^{-1} (LOD = 3 S/m) was achieved for the first time using DMT-AgNPs by spectrofluorimetry. The Stern–Volmer constant value showed the strong quenching

interaction between Hg(II) and DMT-AgNPs. The present method was utilized to determine Hg(II) in environmental samples. The obtained results were compared with ICP-AES method. To the best of our knowledge, this is the first report for the lowest detection with highest selectivity for Hg(II) in aqueous medium using DMT-AgNPs by spectrofluorimetry method.

Acknowledgements

Financial support from Defense Research Development Organization (No. ERIP/ER/0730367/M/01/1132), New Delhi is greatly acknowledged. NV thanks the University Grants Commission, New Delhi, for the award of Meritorious Student Fellowship.

Appendix A. Supplementary data

Supplementary data associated with this article can be found, in the online version, at doi:10.1016/j.jhazmat.2012.01.079.

References

[1] C. Burda, X. Chen, R. Narayanan, M.A. El-Sayed, Chemistry and properties of nanocrystals of different shapes, Chem. Rev. 105 (2005) 1025–1102.
[2] C.J. Murphy, T.K. Sau, A.M. Gole, C.J. Orendorff, J. Gao, L. Gou, S.E. Hunyadi, T. Li, Anisotropic metal nanoparticles: synthesis, assembly and optical applications, J. Phys. Chem. B 109 (2005) 13857–13870.
[3] K-S. Lee, M.A. El-Sayed, Gold and silver nanoparticles in sensing and imaging: sensitivity of plasmon response to size, shape, and metal composition, J. Phys. Chem. B 110 (2006) 19220–19225.
[4] G. Maduraiveeran, R. Ramaraj, Potential sensing platform of silver nanoparticles embedded in functionalized silicate shell for nitroaromatic compounds, Anal. Chem. 81 (2009) 7552–7560.
[5] B.K. Jena, C.R. Raj, Gold nanoelectrode ensembles for the simultaneous electrochemical detection of ultratrace arsenic, mercury and copper, Anal. Chem. 80 (2008) 4836–4844.
[6] R.K. Bera, A.K. Das, C.R. Raj, Enzyme-cofactor-assisted photochemical synthesis of Ag nanostructures and shape-dependent optical sensing of Hg(II) ions, Chem. Mater. 22 (2010) 4505–4511.
[7] B. Adhikari, A. Banerjee, Facile synthesis of water-soluble fluorescent silver nanoclusters and Hg(II) sensing, Chem. Mater. 22 (2010) 4364–4371.
[8] J. Zhang, X. Li, X. Sun, Y. Li, Surface enhanced Raman scattering effects of silver colloids with different shapes, J. Phys. Chem. B 109 (2005) 12544–12548.
[9] I. Onyido, A.R. Norris, E. Buncel, Biomolecule-mercury interaction: modalities of DNA base-mercury binding mechanism. Remediation strategies, Chem. Rev. 104 (2004) 5911–5929.
[10] N. Vasimalai, S.A. John, Ultrasensitive and selective spectrofluorimetric determination of Hg(II) using a dimercaptothiadiazole fluorophore, J. Lumin. 131 (2011) 2636–2641.
[11] D.W. Boening, Ecological effects transport and fate of mercury: a general review, Chemosphere 40 (2000) 1335–1351.
[12] M. Aschner, J.L. Aschner, Mercury neurotoxicity: mechanisms of blood-brain barrier, Neurosci. Biobehav. Rev. 14 (1990) 169–176.
[13] K.V. Gopal, Neurotoxic effects of mercury on auditory cortex networks growing on microelectrode arrays: a preliminary analysis, Neurotoxicol. Teratol. 25 (2003) 69–76.
[14] U.S Environmental protection agency national primary drinking water standards, EPA816-F-01-007, Washington, DC, EPA, 2001.
[15] Guidelines for drinking water quality, vol. 5, 2nd ed., World Health Organization, Geneva, 1996, p. 940.
[16] Y. Wang, F. Yang, X. Yang, Colorimetric detection of mercury (II) ion using unmodified silver nanoparticles and mercury-specific oligonucleotide, ACS Appl. Mater. Interfaces 2 (2010) 339–342.
[17] T. Lou, Z. Chen, Y. Wang, L. Chen, Blue-to-red colorimetric sensing strategy for Hg^{2+} and Ag^{+} via redox-regulated surface chemistry of gold nanoparticles, ACS Appl. Mater. Interfaces 3 (2011) 1568–1573.
[18] E.Y. Hashem, Spectrophotometric studies on the simultaneous determination of cadmium and mercury with 4-(2-pyridylazo)-resorcinol, Spectrochim. Acta A 58 (2002) 1401–1410.
[19] A. Krata, W. Jedral, E. Bulska, On the uniforming process for inorganic and inorganic mercury in graphite furnace atomic absorption spectrophotometry, Spectrochim. Acta B 62 (2007) 269–272.
[20] A.M. Ashrafi, K. Vytras, Stripping voltammetric determination of mercury(II) at antimony-coated carbon paste electrode, Talanta 85 (2011) 2700–2702.
[21] X. Zhu, D.S. Alexandratos, Determination of trace levels of mercury in aqueous solutions by inductively coupled plasma atomic emission spectrometry: elimination of memory effect, Microchem. J. 86 (2007) 37–41.
[22] L. Prodi, Luminescent chemosensors: from molecules to nanoparticles, New J. Chem. 29 (2005) 20–31.
[23] L. Prodi, F. Bolletta, M. Montalti, N. Zaccheroni, Luminescent chemosensor for transition metal ions, Coord. Chem. Rev. 205 (2000) 59–83.
[24] X. Chen, S-W. Nam, M.J. Jou, Y. Kim, S-J. Kim, S. Park, J. Yoon, Hg^{2+} selective fluorescent and colorimetric sensor: its crystal structure and application to bioimaging, Org. Lett. 10 (2008) 5235–5238.
[25] N. Wanichacheva, P. Kumsorn, R. Sangsuwan, A. Kamkaew, V.S. Lee, K. Grudpan, A new fluorescent sensor bearing three dansyl fluorophores for highly sensitive and selective detection of mercury(II) ions, Tetrahedron Lett. 52 (2011) 6133–6136.
[26] H.N. Kim, S-W. Nam, K.M.K. Swamy, Y. Jin, X. Chen, Y. Kim, S-J. Kim, S. Park, J. Yoon, Rhodamine hydrazone derivatives as Hg^{2+} selective fluorescent and colorimetric chemosensors and their applications to bioimaging and microfluidic system, Analyst 136 (2011) 1339–1343.
[27] M. Koneswaran, R. Narayanaswamy, Mercaptoacetic acid capped CdS quantum dots as fluorescence single shot probe for mercury(II), Sens. Actuators B 133 (2009) 91–96.
[28] J.Y. Kwon, J.H. Soh, Y.J. Yoon, J. Yoon, Highly effective fluorescent sensor for Hg^{2+} in aqueous solution, Supramol. Chem. 16 (2004) 621–624.
[29] Y. Cho, S.S. Lee, J.H. Jung, Recyclable fluorimetric and colorimetric mercury-specific sensor using porphyrin-functionalized Au@SiO_2 core/shell nanoparticles, Analyst 135 (2010) 1551–1555.
[30] M.C. Paau, C.K. Lo, X. Yang, M.M.F. Choi, Synthesis of 1.4 nm α-cyclodextrin-protected gold nanoparticles for luminescence sensing of mercury(II) with picomolar detection limit, J. Phys. Chem. C 114 (2010) 15995–16003.
[31] C. Jiang, Z. Guan, S. Yin, R. Lim, L. Polavarapu, Q-H. Xu, Two-photon ratiometric sensing of Hg^{2+} by using cysteine functionalized Ag nanoparticles, Nanoscale 3 (2011) 3316–3320.
[32] X. Peng, Y. Wang, X. Tang, W. Liu, Functionalized magnetic core-shell Fe_3O_4@SiO_2 nanoparticles as selectivity-enhanced chemosensor for Hg(II), Dyes Pigments 91 (2011) 26–32.
[33] N-B. Zhang, J-J. Xu, C-G. Xue, Core–shell structured mesoporous silica nanoparticles equipped with pyrene-based chemosensor: synthesis, characterization, and sensing activity towards Hg(II), J. Lumin. 131 (2011) 2021–2025.
[34] Q.-Y. Chen, C.-F. Chen, A new Hg^{2+} selective fluorescent sensor based on dansyl amide-armed calyx[4]-aza-crown, Tetrahedron Lett. 46 (2005) 165–168.
[35] J. Xie, Y. Zheng, J.Y. Ying, Highly selective and ultrasensitive detection of Hg^{2+} based on fluorescence quenching of Au nanoclusters by Hg^{2+}–Au^{+} interactions, Chem. Commun. 46 (2010) 961–963.
[36] P. Kannan, S.A. John, Synthesis of mercaptothiadiazole-functionalized gold nanoparticles and their self assembly on Au substrates, Nanotechnology 19 (2008) 85602–85612.
[37] P. Kalimuthu, S.A. John, Studies on ligand exchange reaction of funtionalized mercaptothiadiazole compounds onto citrate capped gold nanoparticles, Mater. Chem. Phys. 122 (2010) 380–385.
[38] B.D. Cullity, Elements of X-ray Diffraction, 2nd ed., Addition-Wesley, Menlo Park, CA, 1978.
[39] R. Sardar, J.S. Shumaker-Parry, Asymmetrically functionalized gold nanoparticles organized in one-dimensional chains, Nano Lett. 8 (2008) 731–736.
[40] Y.R. Kim, R.K. Mahajan, J.S. Kim, H. Kim, Highly sensitive gold nanoparticles-based colorimetric sensing of mercury(II) through simple ligand exchange reaction in aqueous media, ACS Appl. Mater. Interfaces 2 (2010) 292–295.
[41] A.T.R. Williams, S.A. Winfield, J.N. Miller, Relative fluorescence quantum yields using a computer-controlled luminescence spectrometer, Analyst 108 (1983) 1067–1071.
[42] J.S. Park, J.N. Wilson, K.I. Hardcastle, U.H.F. Burnz, M. Srinivasarao, Reduced fluorescence quenching of cyclodextrin-acetylene dye rotaxanes, J. Am. Chem. Soc. 128 (2006) 7714–7715.
[43] Q. Zhou, T.M. Swager, Fluorescent chemosensors based on energy migration in conjugated polymers: the molecular wire approach to increased sensitivity, J. Am. Chem. Soc. 117 (1995) 12593–12602.
[44] G. Weber, L.B. Young, Fragmentation of bovine serum albumin by pepsin, J. Biol. Chem. 239 (1964) 1415–1423.
[45] L.D. Ward, Measurement of ligand binding to proteins by fluorescence spectroscopy, Methods Enzymol. 117 (1985) 400–414.
[46] T.J. Dickorson, N.N. Reed, J.J. Laclair, K.D. Janda, A precipitator for the detection of thiophilic metal in aqua, J. Am. Chem. Soc. 126 (2004) 16582–16586.
[47] M.H. Lee, S.W. Lee, S.H. Kim, C. Kim, J.-S. Kim, Nanomolar Hg(II) detection using nile blue chemotosimites in biological media, Org. Lett. 11 (2009) 2101–2104.
[48] C.-J. Yu, W.L. Tseng, Colorimetric detection of mercury (II) in a high salinity solution using gold nanoparticles capped with 3-mercaptopropionate acid and adenosine monophosphate, Langmuir 24 (2008) 12717–12722.